Mean-square-displacement distribution in crystals and glasses: An analysis of the intrabasin dynamics

Hugo M. Flores-Ruiz and Gerardo G. Naumis

Instituto de Física, Universidad Nacional Autónoma de México (UNAM), Apartado Postal 20-364, 01000, México, Distrito Federal, Mexico

(Received 20 October 2011; revised manuscript received 29 March 2012; published 18 April 2012)

In the energy landscape picture, the dynamics of glasses and crystals is usually decomposed into two separate contributions: interbasin and intrabasin dynamics. The intrabasin dynamics depends partially on the quadratic displacement distribution on a given metabasin. Here we show that such a distribution can be approximated by a Gamma function, with a mean that depends linearly on the temperature and on the inverse second moment of the density of vibrational states. The width of the distribution also depends on this last quantity, and thus the contribution of the boson peak in glasses is evident on the tail of the distribution function. It causes the distribution of the mean-square displacement to decay slower in glasses than in crystals. When a statistical analysis is performed under many energy basins, we obtain a Gaussian in which the width is regulated by the mean inverse second moment of the density of states. Simulations performed in binary glasses are in agreement with such a result.

DOI: 10.1103/PhysRevE.85.041503 PACS number(s): 64.70.Q−, 64.70.kj, 61.43.Fs

I. INTRODUCTION

Humanity began making amorphous solids hundreds of years ago [1,2]. Window glass is the best known example of an amorphous solid, but there are many others used in devices such as silicon photovoltage cells, optical fibers, and so on [2]. In spite of such widespread use of glasses, their formation process is still controversial [2–4]. To understand the formation of glasses and crystals, as well as the dynamics of supercooled liquids [5], it is common to use the energy landscape picture [6]. This landscape is a multidimensional surface generated by the system potential energy as a function of the molecular coordinates [1,2,7,8]. In an N-body system, it is determined by the potential energy function, given by $\phi(\mathbf{r}_1, \ldots, \mathbf{r}_N)$, where $\mathbf{r}_i$ comprise all configuration coordinates. Once a glass is formed, it shares a basic attribute with a crystal at low temperature: both represent a minimum [1,8] in ϕ. Perfect crystals correspond to an absolute minimum in ϕ, while amorphous crystals are in relatively higher metastable states. These minima are called inherent structures (ISs) [1]. Most of the works concerning glass formation analyze the dynamics of the glass-forming liquid in the supercooled region [1,8–11]. Commonly, such dynamics is separated into two contributions: transitions between ISs and vibrational motion into each energy basin of a given IS [1,7,8]. In other words, the dynamics is separated into short times (vibrations and transitions to minima separated by very low energy barriers) and long times [2,12–14] (relaxation due to transitions into ISs), as was tested by Schroder *et al*. [10] and Broderix *et al*. [15]. Furthermore, the long-time dynamics in low-temperature model supercooled liquids has been found to be related with a hierarchy in the ISs, since it is possible to cluster them in metabasins (MB) [16–20], a feature that is reminiscent of the funnel structure of the energy landscape in proteins. In fact, the glassy landscape can be decomposed into an exponential number of local funnels, resulting in a highly frustrated structure. Thus the dynamics can be represented by a random walk between traps with a certain waiting time distribution [17,19,20]. In such an approach, called the trap model [20], one needs to separate the vibrational dynamics from the long-time behavior. Usually, the vibrational component of the trajectory is separated through quenching to ISs, assuming that the vibrational component can be removed. Then the trajectory between ISs is kept. A different approach is obtained by identifying a network composed of transition states and the minima they connect [21,22]. When basins refer to individual local minima, this method allows us to separate local vibrational modes and transitions between minima. Recently, a clear criterion to define MBs has been identified, where changes between MB are due to *productive* cage-breaking events [23,24]. These events are defined by nonreversible changes of at least two neighbors for any atom. The criterion to decide which are the neighbors depends upon a critical distance (R_c), chosen from the radial distribution function [23]. It turns out that these events are in clear correspondence with the MBs found using a metrics defined as the "distance" between ISs [23]. Clearly, the mean square displacement fluctuations are useful for looking at the possibility of cage breaking [25], since at least two displacements must have a magnitude bigger than a certain threshold. Thus, it is worthwhile to study such fluctuations. In this article, we will examine this point by analyzing the vibrational component statistics. In particular, we will consider the mean square displacement at its plateau level ($\overline{u^2}$) fluctuations.

Thus, here we will need to calculate the distribution function $P(\overline{u^2}; l)$ of $\overline{u^2}$, where l is a label for the energy basin. Since one of the most intriguing questions on glasses is why the short-time scale behavior, given by the properties of $\overline{u^2}$, can be used to predict the long-time behavior [26,27], the knowledge of $P(\overline{u^2}; l)$ can also be used to shed some light on the problem. Also, we will discuss its relationship with the total probability density over different inherent structures $P(\overline{u^2})$, and the mean square displacement $\langle \overline{u^2} \rangle_l$ and $\langle u^2 \rangle$ obtained from the first moment of $P(\overline{u^2}; l)$ and $P(\overline{u^2})$, respectively.

It is worthwhile mentioning that the vibrational time scale corresponds to cage effects [23,28], and thus to a plateau for $\overline{u^2}$. Following this idea, we can study the mechanical

stability for temperatures below the melting point (T_m) or glass transition temperature (T_g). Recently, we have shown that in fact, the glass transition temperature as well as the viscosity are determined by $\langle\overline{u^2}\rangle$ [29–36]. In such a deduction, we observed that the excess of low-frequency vibrational modes (LFVMs) [37,38] present in glasses leads to a bigger $\langle\overline{u^2}\rangle$ when compared to crystals, explaining why T_g is always below T_m. Furthermore, glasses present two anomalies in the reduced vibrational density of states (RVDOS) [39]: One is associated with the excess of LFVMs, dubbed the boson peak (BP), which is over finite tera-hertz frequencies (ω) [38]. The other one is called the floppy peak (FP), which appears at ω close to zero [40]. The latter case is explained by means of the floppy mode concept that was introduced by Phillips-Thorpe's rigidity theory (RT) [41–44]. Basically, floppy modes arise in atomic networks with low coordination [40]. Recently, it has been suggested that the BP and FP have a common origin, *a lack of contacts* [39]. This fact has been observed experimentally in [45]. Namely, a BP occurs as a consequence of a reduction of constrictions in an overconstrained lattice, while the FP appears due to a reduction of contacts in an isostatic network [39].

Finally, in this article we want to make a connection between anomalous LFVMs and the probability distributions functions $P(\overline{u^2};l)$ and $P(\overline{u^2})$ in crystals and glasses, and their relationship with the interbasin and intrabasin dynamics. Notice that some of the short-time dynamics is not just vibrational since transitions between local minima also occur with low barriers, as has been observed in computer simulations [23,24]. Our method, in principle, cannot distinguish between them, since we assume harmonic oscillations right from the beginning. In spite of this, the well known fact that in real glasses long-time properties are given by short-time vibrational properties hints at the fairness of the procedure [26,27]. Maybe this is due to a nearly similar local topology between ISs separated by low energy barriers.

This work is organized as follows. In Sec. II, we present a discussion on the energy landscape dynamics and some molecular dynamics simulations (MD) which were used to compare with our theoretical results, developed in Sec. III. The conclusions are given in Sec. IV.

II. SQUARE DISPLACEMENT AND INHERENT STRUCTURES IN BINARY GLASSES

The proposal of this section is twofold. First, we want to present how $\overline{u^2}$ is related with the energy basin in simulations concerning binary glasses, and second, we want to show the protocol of the simulations that were made in order to corroborate our theoretical outcome. As our system, we used an 80:20 mixture glass of A and B particles. For crystals, we used a face-centered-cubic (fcc) crystal made only with A particles. This choice is due to the fact that for the A-B system, the lowest-energy non-phase-separated state is not fcc for a binary Lennard-Jones potential [46,47]. However, here we are only concerned with testing our theoretical distribution for glasses and crystals, thus one can use any arbitrary crystal to make the corresponding check.

In both cases, all particles have the same mass m. The interactions between particles are given by a purely repulsive potential [48],

$$\phi_{\alpha\beta}(r_{ij}) = \begin{cases} 4\epsilon_{\alpha\beta}\left[\left(\frac{\sigma_{\alpha\beta}}{r_{ij}}\right)^{12} - \left(\frac{\sigma_{\alpha\beta}}{r_{ij}}\right)^{6}\right] + \epsilon_{\alpha\beta} & \text{if } r_{ij} \leqslant r_{\alpha\beta}^{c} \\ 0 \quad \text{in any other case,} \end{cases} \tag{1}$$

where r_{ij} is the interparticle distance, $\epsilon_{\alpha\beta}$ is a constant energy, and $r_{\alpha\beta}^{\text{cut}} = 2^{1/6}\sigma_{\alpha\beta}$ is the cutoff radius. The units of mass, length, time, pressure, and temperature are m, σ_{AA}, $\tau = \sigma_{AA}\sqrt{m/\epsilon_{AA}}$, $\epsilon_{AA}/\sigma_{AA}^3$, and ϵ_{AA}/k_B, respectively, with k_B being Boltzmann's constant. The glass simulation parameters $\epsilon_{\alpha\beta}^g$ and $\alpha_{\alpha\beta}^g$ were chosen as follows to inhibit crystallization [48]: $\sigma_{AA}^g = 1.0$, $\epsilon_{AA}^g = 1.0$, $\sigma_{AB}^g = 0.88$, $\epsilon_{AB}^g = 1.5$, $\sigma_{BB}^g = 0.8$, and $\epsilon_{BB}^g = 0.5$. The length box was $L^g/\sigma_{AA}^g = 8.4852$. The glass was produced by supercooling [48]: we heated a doped simple-cubic (sc) crystal up to fluid state, and then we cooled it at speed $\gamma_- = dT/dt = 0.2$ until it was in a solid amorphous state. Once the glass was obtained, the initial configuration was heated at the heating rate $\gamma = 0.005$. Meanwhile, the monodispersive crystal simulation was performed with the following parameters: $\sigma_{AA}^c = 1.0$, $\epsilon_{AA}^c = 1.0$, $\sigma_{AB}^c = 1.0$, $\epsilon_{AB}^c = 1.0$, $\sigma_{BB}^c = 1.0$, $\epsilon_{BB}^c = 1.0$ and length box $L^c/\sigma_{AA}^c = 9.5244$ with the same repulsive potential (1). The simulations were made with $N = 864$ particles at constant volume and temperature. All quantities reported in this paper are in dimensionless molecular dynamics units.

An interesting question is why we chose a purely repulsive potential. The answer to this question has to do with the possibility of relating the boson peak with the mean-square displacement (MSD) and rigidity. The use of a purely repulsive potential with a given cutoff allows us to define unambiguously when particles have constraints and how to count them [49]. As we will see, the MSD distribution is basically defined from the low-frequency modes, and thus constraints play a major role, as we shown in Ref [49].

Once the glasses and crystals were obtained, an analysis of the statistical properties of the MSD was performed. The MSD, $u^2(t)$, is an average over all particles at a given time,

$$u^2(t) = \frac{1}{N}\sum_{j=1}^{N}\mathbf{u}_j^2 = \frac{1}{N}\sum_{j=1}^{N}[\mathbf{r}_j(t) - \bar{\mathbf{r}}_j]^2, \tag{2}$$

where $\mathbf{u}_j$ is the particles' displacement, $\mathbf{r}_j(t)$ is the position, and $\bar{\mathbf{r}}_j$ is the average position after a time $\mathcal{T}$,

$$\bar{\mathbf{r}}_j = \frac{1}{\mathcal{T}}\int_0^{\mathcal{T}}\mathbf{r}_j(t)\,dt. \tag{3}$$

If $u^2(t)$ reaches a plateau after a certain time t_1, we define a stochastic variable $\overline{u^2}$ whose values are given by the sequence

$$\overline{u^2} = u^2(t), \tag{4}$$

where t is inside a time interval $t_1 < t < t_2$ such that $u^2(t_2)$ is still in the same plateau.

In the case of the relaxed crystal, the distribution $P_c(\overline{u^2};l)$ is equal to $P_c(\overline{u^2})$ since the system is in the absolute minimum of ϕ and $\bar{\mathbf{r}}_j$ corresponds to the mechanical equilibrium position. Then we can obtain $P_c(\overline{u^2})$ just by doing the statistics of $\overline{u^2}$

during a given amount of time $t_2 - t_1$. The results are going to be discussed in the next section and are presented in Fig. 3.

For glasses, the probability distribution over different energy basins $P_g(\overline{u^2};l)$ warrants some important remarks:

(i) The system can jump between IS and metabasins, and u^2 can have many or any jumps.

(ii) Such jumps produce huge changes in $\overline{\mathbf{r}}_j$ as $\mathcal{T} \to \infty$.

(iii) One can only do statistics for $\overline{u^2}$ during the lifetime on each basin $[\tau(l)]$, where l labels the basin.

To keep track of changes in $\overline{\mathbf{r}}_j$ when a hop to a new basin occurs, we replace $\overline{\mathbf{r}}_j$ by $\mathbf{R}_j(t)$, where $\mathbf{R}_j(t)$ is the coordinate of particle j in the new IS at time t. Therefore we have two distributions, one over a given basin denoted by $P(\overline{u^2};l)$ and one over all basins $P_g(\overline{u^2})$, as stated previously. On both cases, the critical step is how to decide when the system leaves a basin. This problem can be tackled if a distance is defined between ISs [9] at each time step,

$$\delta\mathbf{R}(t) = \sqrt{\frac{1}{N}\sum_{j=1}^{N}[\mathbf{R}_j(t) - \mathbf{R}_j(t-\Delta t)]^2}. \tag{5}$$

Ideally, one should obtain $\delta\mathbf{R}(t) \neq 0$ only when a change of IS occurs. However, $\delta\mathbf{R}(t)$ also follows a distribution [9]. Therefore, $\delta\mathbf{R}(t)$ is almost always different from zero. To solve this problem, a minimal cutoff in $\delta\mathbf{R}_0$ is needed in order to discriminate between small and big jumps. In the present case, we used a steepest-descent algorithm to search for the IS while looking at $u^2(t)$. In Fig. 1, we plot $u^2(t)$ against time for different cutoffs ($\delta\mathbf{R}_0$). Notice how the value of $u^2(t)$ is reset to zero once a change in the inherent structure is detected with a given cutoff, as shown in the figure for $\delta\mathbf{R}_0 = 0.45, 0.55, 0.65, 0.75$. Clearly, $u^2(t)$ never reaches a plateau if $\delta\mathbf{R}_0$ is very small. Thus, the criterion is to look for a minimal value of $\delta\mathbf{R}_0$ able to produce plateaus in $u^2(t)$. Then statistics of $\overline{u^2}$ can be measured for each visited inherent structure. This is in agreement with the idea of separating the energy landscape into a hierarchical structure, where some rearrangements are minimal compared with large but rare changes. In fact, our criterion is akin to the MB concept investigated by Heuer and co-workers [16,17,19], where ISs are grouped into MBs. ISs in the same MB are found by looking to a distance matrix [18], akin to Eq. (5). For example, Appignanesi *et al.* [18] found that the quadratic distance between MBs is around 0.06 for $T = 0.50$, close to the value $\delta\mathbf{R}_0^2 \approx (0.85)^2 = 0.72$ found by us in a similar temperature. The cutoff $\delta\mathbf{R}_0$ depends on the temperature, and eventually it is impossible to obtain plateaus, as expected. However, below T_g we observed that such separation is possible, but it requires a fine tuning of $\delta\mathbf{R}_0$. Since Eq. (5) is akin to the distance matrix method, our identification of MBs produces similar results to those obtained from the identification of the transition and minima network using disconnectivity graphs [23,24].

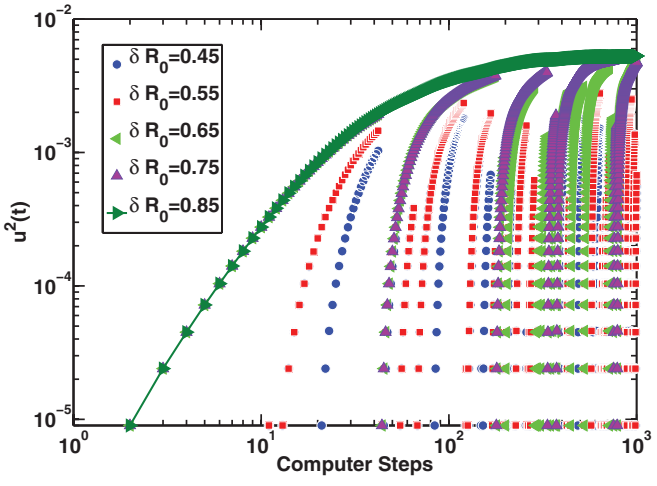

FIG. 1. (Color online) MSD as a function of the computer time using different cutoffs to separate inherent structures in a glass at $T = 0.5$. As explained in the inset, each symbol represents a different cutoff criteria chosen to distinguish small and big jumps between ISs. A reset of the MSD occurs whenever a change in the inherent structure is detected with the given cutoff, since the system hops to a new basin. In the example, it is impossible for the MSD to reach a plateau for $\delta\mathbf{R}_0 < 0.85$. This value is similar to the one obtained using the distance matrix method [18].

In what follows, by different energy basins we will be referring to those that have a $\delta\mathbf{R} > \delta\mathbf{R}_0$, since they correspond to different MBs. As a result, all of our averages over IS are performed over MBs. The distribution of waiting time on MBs has been well documented [16,17,19], with a mean dominated by contributions from large waiting times [17]. The possibility of having a plateau in $u^2(t)$ depends on the time scale for ballistic behavior and the mean waiting time on MBs. In fact, it is interesting to ask when the time average of $u^2(t)$ at a given short time ς,

$$\langle u^2\rangle = \frac{1}{\varsigma}\int_0^{\varsigma} u^2(t)dt, \tag{6}$$

calculated during many time windows, can be equal to the average of $\overline{u^2}$ over IS with a cutoff $\delta\mathbf{R}_0$. In Fig. 2, we compare the results using Eq. (6) for short times, the average of $\overline{u^2}$ in

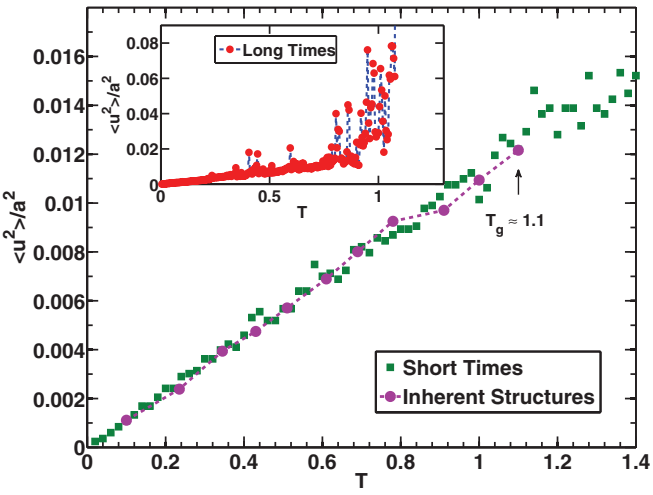

FIG. 2. (Color online) $\langle u^2\rangle$ normalized by the average interatomic distance as a function of the temperature using averages over short times, and averages of $\overline{u^2}$ on IS. Inset: the same but using long times in Eq. (2). T_g is indicated and corresponds to $\langle u^2\rangle/a^2 \approx 0.012$, which is close to the Lindemann ratio. T_g was obtained from the radial distribution function, internal energy, and specific heat [49].

IS (denoted as $\langle\overline{u^2}\rangle$), and for long times. In this simulation, T_g is shown with an arrow; its value was obtained by looking at the radial distribution function, the internal energy, and the specific heat, as explained in Ref. [49]. One can see that the results from short times and ISs are similar below T_g, while for long times the behavior is not smooth and nonconvergent, as expected. After T_g, it is difficult to extract a meaningful $\langle\overline{u^2}\rangle$ using the IS criterion. However, two interesting conclusions are obtained from Fig. 2:

(i) $\langle u^2\rangle$ and $\langle\overline{u^2}\rangle$ are linear in T, indicating harmonic behavior on each MB [35].

(ii) T_g follows Lindemann's criterion where $\sqrt{\langle u^2\rangle} \approx 0.1a$, and thus it is very difficult to separate the vibrational and intrabasin dynamics beyond T_g, at least for this soft glass.

In the following section, we will discuss the MSD distribution on crystals and in a given energy basin.

III. DISTRIBUTION FUNCTION OF THE SQUARED DISPLACEMENT IN AN ENERGY BASIN

As explained before, here we are interested in the square displacement $\overline{u^2}$ and its distribution function $P(\overline{u^2};l)$ for crystals and glasses in a basin l. Assuming a harmonic approximation, consider a network of N point particles with mass $m = 1$ and connected by springs in a space of dimension D. The potential part of the Hamiltonian in the harmonic approach is

$$E = \frac{1}{2}\sum_{ij} k_{ij}[(\mathbf{u}_i - \mathbf{u}_j)\cdot\hat{\mathbf{n}}_{ij}]^2, \tag{7}$$

where $\mathbf{u}_j$ and $\mathbf{u}_i$ are the particles' displacement, $\hat{\mathbf{n}}_{ij}$ is the unitarian vector between such elements, and k_{ij} is the second-order derivative of the harmonic potential. It is convenient to express Eq. (7) in matrix form, defining the set of displacements $\mathbf{u}_1,\ldots,\mathbf{u}_j$ as a DN dimensional vector $\mathbb{U}$. Equation (7) can be written in the form

$$E = \tfrac{1}{2}\mathbb{U}^T\mathbb{M}\mathbb{U}, \tag{8}$$

where $\mathbb{M}$ is the corresponding $DN \times DN$ dynamical matrix [50] whose elements are $\mathbb{M}_{ij} = \delta_{ij}\sum_l k_{il}\hat{\mathbf{n}}_{il}\otimes\hat{\mathbf{n}}_{il} - k_{ij}\hat{\mathbf{n}}_{ij}\otimes\hat{\mathbf{n}}_{ij}$. As is well known, we can apply a linear transformation, $\mathbb{U} = \mathbb{A}\mathbb{Q}$, to diagonalize [51] Eq. (8),

$$E = \frac{1}{2}\mathbb{Q}^T\mathbb{O}\mathbb{Q} = \frac{1}{2}\sum_{j=1}^{DN}\omega_j^2 Q_j^2. \tag{9}$$

In this expression, $\mathbb{O} = \mathbb{A}^T\mathbb{M}\mathbb{A}$, a $DN \times DN$ matrix, contains the square normal frequencies $\omega_1^2,\ldots,\omega_{DN}^2$ and the vector $\mathbb{Q}$ contains the set of normal mode coordinates $Q_1,\ldots,Q_{DN}$. We can obtain the square displacement per particle as

$$\overline{u^2} = \frac{1}{N}\mathbb{U}^T\mathbb{U} = \frac{1}{N}\mathbb{Q}^T\mathbb{A}^T\mathbb{A}\mathbb{Q} = \frac{1}{N}\mathbb{Q}^T\mathbb{Q} = \overline{Q^2}. \tag{10}$$

Behind this result there is a clear mathematical fact: $\overline{u^2}$ is the norm of a DN-sized vector in configurational space and is an invariant under rotations, as is the one induced by the linear transformation $\mathbb{A}$.

In this way, $P(\overline{u^2};l)$ is the distribution function of the sum of DN square random variables. This problem has a long history and still is a subject of research by mathematicians [52–56]. However, their resulting expressions are quite complicated and without a clear physical context; here we want to find an expression for $P(\overline{u^2};l)$ with a physical background. For the particular case of an Einstein solid, the result is simple, since all normal modes are at the same frequency ω_0, and,

$$P_{EC}(\overline{u^2}) = \frac{[N]^{DN/2}}{\Gamma(DN/2)\sigma_1^{DN/2}}[\overline{u^2}]^{DN/2-1}e^{-N\frac{\overline{u^2}}{2\sigma_1^2}} \tag{11}$$

with $\sigma_1^2 = k_BT/\omega_0^2$, and mean and variance given by

$$\langle\overline{u^2}\rangle_{EC} = \frac{Dk_BT}{\omega_0^2} \quad \text{and} \tag{12}$$

$$\Sigma_{EC}^2 = \frac{2D\,(k_BT)^2}{N\omega_0^4}, \tag{13}$$

respectively.

In a general case, we will calculate $P(\overline{u^2};l)$ from the distribution of displacements of the normal modes $P(\overline{Q^2};l)$, since from Eq. (10), $\overline{u^2} = \overline{Q^2}$, $P(\overline{u^2};l) = P(\overline{Q^2};l)$.

Under the assumption of being in a metastable or stable state, according to the Gibbs distribution [57] and Eq. (9), the distribution function of $P(Q_j)$ is a Gaussian,

$$P(Q_j) = \frac{1}{\sqrt{2\pi}\sigma_j}e^{-Q_j^2/2\sigma_j^2}, \tag{14}$$

where $\sigma_j^2 = k_BT/\omega_j^2$. Equation (14) is very important because it gives the distribution function $P(Q_j^2)$, due to the fact that $P(Q_j^2)dQ_j^2 = P(Q_j)dQ_j$. It is better to define a variable $Y_j \equiv Q_j^2/N$, write $\overline{u^2}$ as $\overline{u^2} = \sum_{j=1}^{DN} Y_j$, and $P(Y_j)$ as

$$P(Y_j) = \frac{1}{\sqrt{2\pi}\widetilde{\sigma_j}\sqrt{Y_j}}e^{-Y_j/2\widetilde{\sigma_j}^2}, \quad Y_j \in [0,\infty), \tag{15}$$

where $\widetilde{\sigma_j}^2 = \sigma_j^2/N$.

With all the previous elements, $P(\overline{u^2};l)$ is in essence the distribution function of the sum of DN random variables Y_j, with median $\widetilde{\sigma_j}^2$ and variance $2\widetilde{\sigma_j}^4$ [54]. Therefore,

$$P(\overline{u^2};l) = \int_0^\infty\cdots\int_0^\infty \delta\left(\overline{u^2} - \sum_{j=1}^{DN} Y_j\right) P(Y_1)\cdots P(Y_{DN}) \times dY_1\cdots dY_{DN}. \tag{16}$$

In this preceding equation, $\delta(\overline{u^2} - \sum_{j=1}^{DN} Y_j)$ is a constriction and $P(Y_j)$ refers to the expression (15). We can use an integral representation of the Dirac δ expression in order to rewrite the constriction,

$$\delta\left(\overline{u^2} - \sum_{j=1}^{DN} Y_j\right) = \frac{1}{2\pi}\int_{-\infty}^{\infty} e^{-iK(\overline{u^2}-\sum_{j=1}^{DN}Y_j)}dK.$$

Inserting this expression and the relation (15) in Eq. (16), we have

$$P(\overline{u^2};l) = \frac{1}{2\pi}\int_{-\infty}^{\infty} e^{-iK\overline{u^2}}\prod_{j=1}^{DN}\Phi_j(K)\,dK, \tag{17}$$

where $\Phi_j(K)$ is a jth generating function, corresponding to the Y_j random variable. Actually, Eq. (17) is a convolution of

DN functions Φ_j, or more explicitly, $P(\overline{u^2};l) = (\Phi_1 * \ldots * \Phi_{DN})(\overline{u^2})$.

The expression for $\Phi_j(K)$ is

$$\Phi_j(K) = \frac{1}{\sqrt{2\pi\widetilde{\sigma}_j}} \int_0^\infty \frac{e^{-Y_j[(2\widetilde{\sigma}_j)^{-1} - iK]}}{\sqrt{Y_j}} dY_j = \frac{1}{[1 - iK2\widetilde{\sigma}_j]^{1/2}}. \tag{18}$$

We expand at second order in K the jth generating function $[1 - iK2\widetilde{\sigma}_j]^{-1/2} \approx 1 + iK\widetilde{\sigma}_j^2 - \frac{3}{2}K^2\widetilde{\sigma}_j^4$. In this way, we perform the product $\prod_{j=1}^{DN}[1 - iK2\widetilde{\sigma}_j]^{-1/2}$ until K^2. Such an approach works better when there is a huge number of DN degrees of freedom, therefore

$$\prod_{j=1}^{DN}[1 - iK2\widetilde{\sigma}_j]^{-1/2} \approx \frac{1}{[1 - iK\sigma_l^2/N]^N}, \tag{19}$$

where $\sigma_l^2 = \sum_{j=1}^{DN} \widetilde{\sigma}_j^2 \approx Dk_BT \int_0^{\omega_{\rm cut}} \rho_l(\omega)/\omega^2 d\omega \equiv Dk_B T\langle\omega^{-2}\rangle_l$ and $\rho_l(\omega)$ is the vibrational density of states in the corresponding energy basin l. Using Eq. (19), we perform the integral (17) and the resulting probability density for $\overline{u^2}$ is

$$P(\overline{u^2};l) \approx \frac{[N]^N}{\Gamma(N)\sigma_l^N}[\overline{u^2}]^{N-1} e^{-N\frac{\overline{u^2}}{\sigma_l^2}}. \tag{20}$$

The distribution given by (20) is a Gamma function [54] with mean $\langle\overline{u^2}\rangle_l$ [35,36,49] and variance Σ_l^2 given by the expressions

$$\langle\overline{u^2}\rangle_l \approx Dk_BT \int_0^{\omega_{\rm cut}} \frac{\rho_l(\omega)}{\omega^2} d\omega \equiv Dk_BT\langle\omega^{-2}\rangle_l \quad \text{and} \tag{21}$$

$$\Sigma_l^2 \approx \frac{(Dk_BT)^2}{N}\left[\int_0^{\omega_{\rm cut}} \frac{\rho_l(\omega)}{\omega^2} d\omega\right]^2 = \frac{\langle\overline{u^2}\rangle_l^2}{N}. \tag{22}$$

The predictions contained in Eqs. (21) and (22) are going to be tested against the simulations once an average over energy basins is performed, as shown in Fig. 5.

It is important to observe that $P(\overline{u^2};l)$ in (20) could also be approximated by a normal distribution $\mathcal{N}(\langle\overline{u^2}\rangle_l, \Sigma_l^2)$ when $N \to \infty$ [55]. However, here we decide to express $P(\overline{u^2};l)$ as a Gamma distribution since its domain is the positive real axis, which is not the case for the Gaussian.

Also, it is worthwhile observing that Eqs. (21) and (22) were derived under the assumption of a long-lived metastable state which allows us to define the lower limit of the integral as $\omega \to 0$. However, is clear that one cannot go below a lower cutoff frequency $\omega_l^* = 2\pi/\tau(l)$, where $\tau(l)$ is the lifetime of the system in the metastable feature l. Thus,

$$\langle\overline{u^2}\rangle_l \approx Dk_BT \int_{2\pi/\tau(l)}^{\omega_{\rm cut}} \frac{\rho_l(\omega)}{\omega^2} d\omega. \tag{23}$$

Now let us analyze the deep physical meanings of Eqs. (21) and (22). First, the linear scaling of $\langle\overline{u^2}\rangle_l$ with T predicted in Eq. (21) is consistent with the computer simulation (see Fig. 2) and has also been reported in other simulations of glasses and crystals [35,36,49] and in experimental data for strong and fragile glasses [58–60].

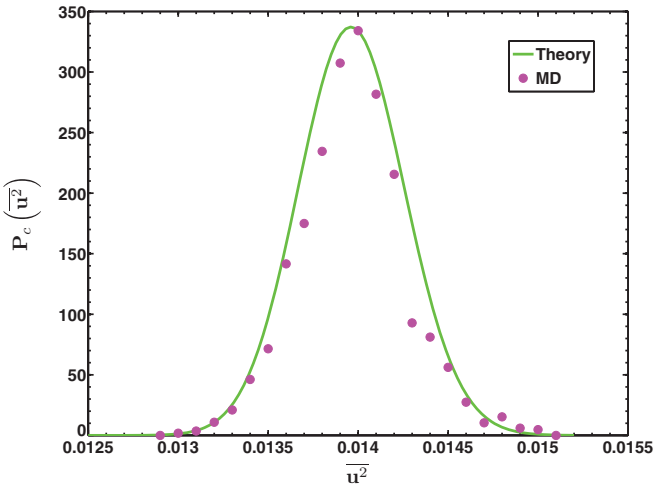

FIG. 3. (Color online) Distribution function $P_c(\overline{u^2})$ in a fcc monocomponent crystal made of A atoms at $T = 0.510$. The continuous green line refers to the fitting using Eq. (20), and the fuchsia points refer to the crystal molecular dynamics simulations with $\langle u^2\rangle_c \approx 1.40 \times 10^{-2}$ and $\sigma_c^2 \approx 8.69 \times 10^{-8}$ at $T = 0.510$.

Second, the mean of the MSD is given by the second inverse moment $\langle\omega^{-2}\rangle_l$ of the density of states. In Eq. (21) it means that low-frequency modes are essential to the stability of the system. In crystals at $T < T_m$, when the quantity $\langle\omega^{-2}\rangle_c$ is analyzed, one obtains an important criterion for the stability [61]. For $D = 1$ or 2, $\langle\omega^{-2}\rangle_c \to \infty$ when $\omega \to 0$. As a consequence, $\langle\overline{u^2}\rangle_c \to \infty$ as well as $\sigma_c^2 \to \infty$. For $D = 3$, $\rho_c(\omega) \sim \omega^2$ and $\langle\omega^{-2}\rangle_c = \text{const}$. Thus, $\langle\overline{u^2}\rangle_c \sim T$ and $\sigma_c^2 \sim T^2$ and three-dimensional crystals turn out to be stable against thermal fluctuations. Figure 3 shows a comparison between $P_c(\overline{u^2})$, Eq. (20), and the results from the molecular dynamics simulation in a fcc monocomponent crystal made of A atoms at $T = 0.510 < T_m$. The agreement between both is very good.

Equations (20)–(22) can be applied to glasses in a range of temperatures in which the harmonic approach works. The boson [2,62] or floppy mode peak on glasses leads to a distribution function $P_g(\overline{u^2};l)$ that differs from that of the crystals in the following ways:

(i) The average of the MSD is shifted to higher values since $\rho_l(\omega)/\omega^2$ has a peak at low frequencies.

(ii) The width of the distribution is increased by the same phenomena.

From the previous analysis, is clear that the common picture of viewing the crystalline state as if it is just a global minimum of ϕ needs to be refined by observing that the local topology of the crystalline minimum and glasses is different, in the sense that the average curvature of the basin is reduced in the former. As a result, there is a higher probability of big displacements.

Finally, Eqs. (21) and (22) depend on the particular MB. This problem can be solved by averaging under ISs, i.e., we define $P_g(\overline{u^2})$, where $\overline{u^2}$ is taken from a representative sample of ISs, chosen using a good cutoff criterion. By representative we mean that the mean and variance of the distribution are convergent. Since we are summing random stochastic variables with different distributions at each basin,

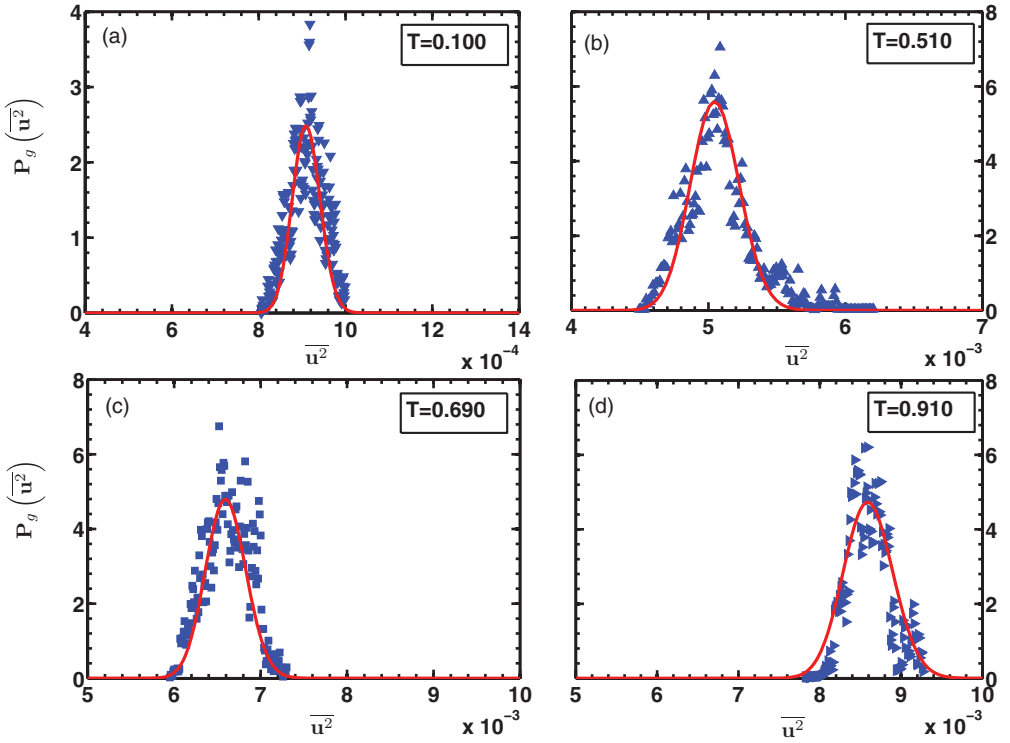

FIG. 4. (Color online) Distribution functions $P_g(\overline{u^2})$ for a binary glass 80:20 at different temperatures. The continuous red line refers to the fitting using the theoretical approach, Eq. (24), and the blue triangles refer to the binary glass molecular dynamics simulations. The heating rate was $\gamma = 0.005$. Notice the scale change as the temperature is raised, indicating wider distributions.

we can use the central limit theorem to obtain a Gaussian distribution,

$$P_g(\overline{u^2}) = \frac{1}{\sqrt{2\pi\sigma_g^2}} e^{-\frac{(\overline{u^2}-\langle\overline{u^2}\rangle_g)^2}{2\sigma_g^2}}, \tag{24}$$

with mean and variance given by

$$\langle\overline{u^2}\rangle_g = \frac{1}{N_l}\sum_l \langle\overline{u^2}\rangle_l = Dk_BT\langle\langle\omega^{-2}\rangle\rangle, \tag{25}$$

$$\sigma_g^2 = \frac{1}{N_l}\sum_l \Sigma_l^2 = \frac{\langle\overline{u^2}\rangle_g^2}{N}, \tag{26}$$

respectively, where

$$\langle\langle\omega^{-2}\rangle\rangle = \frac{1}{N_l}\sum_l \int_{2\pi/\tau(l)}^{\omega_{\rm cut}} \frac{\rho_l(\omega)}{\omega^2} d\omega \approx \int_0^{\omega_{\rm cut}} \frac{\overline{\rho(\omega)}}{\omega^2} d\omega. \tag{27}$$

To test this idea, a MD simulation was performed in order to obtain the distribution function of $\overline{u^2}$ in a binary glass 80 : 20 using the procedures described in Sec. II. In Fig. 4, we present a comparison between the numerical binary glass probability density distribution $P_g(\overline{u^2})$ at different temperatures and Eq. (24). One can observe that the mean of each distribution is displaced as the temperature is raised, and at the same time the distributions become wider. The key to a more quantitative comparison of the obtained distributions and the simulations is to show that the mean and variance of $P_g(\overline{u^2})$ are really given by Eqs. (25) and (26). To test this, in Fig. 5 we present the mean of $P_g(\overline{u^2})$ compared to $3k_BT\langle\langle\omega^{-2}\rangle\rangle$, which was obtained from $\rho(\omega)$ through the velocity-velocity correlation, as explained in Ref. [49]. Both are linear on T, as predicted, and the slope is similar, although the line defined by $3k_BT\langle\langle\omega^{-2}\rangle\rangle$ is steeper. Such a discrepancy can be due to the presence of nonlinear

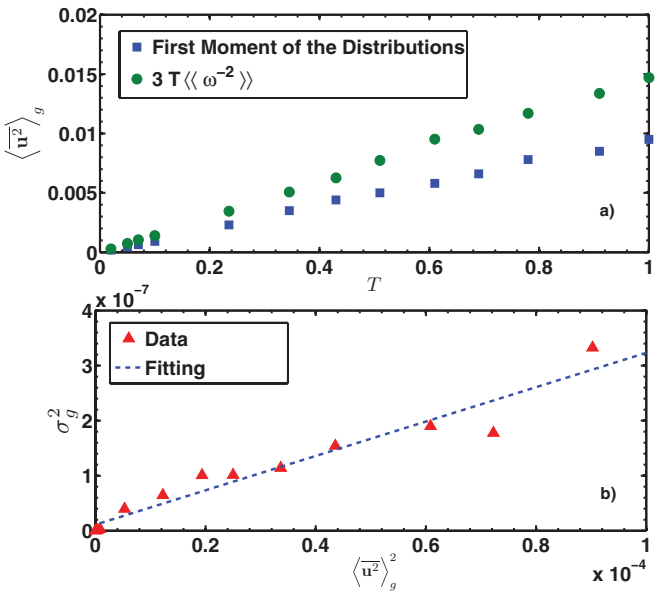

FIG. 5. (Color online) Upper plot: mean of $P_g(\overline{u^2})$ as a function of the temperature, compared with $3T\langle\langle\omega^{-2}\rangle\rangle$ as obtained from the density of vibrational states. Lower plot: a comparison of the $P_g(\overline{u^2})$ variance against $\langle\overline{u^2}\rangle_g^2$. The upper plot validates Eq. (25), while the lower plot validates Eq. (26).

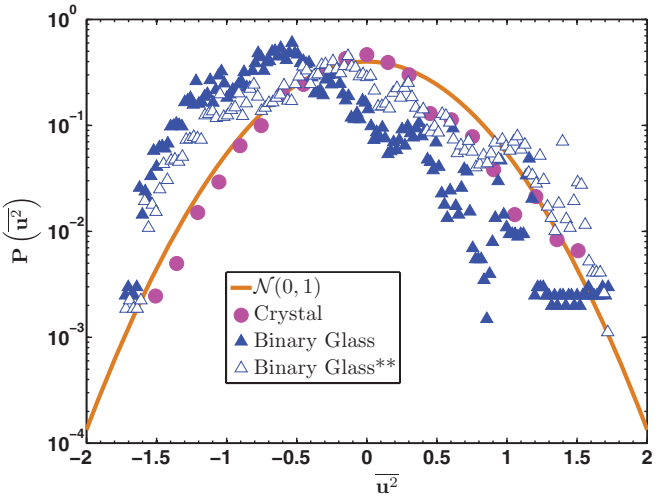

FIG. 6. (Color online) Normalized distribution function of $\overline{u^2}$ in a semilog scale. The continuous orange line refers to the normal distribution $\mathcal{N}(0,1)$. The fuchsia points represent the crystal simulations at $T = 0.510$, while the solid blue triangles represent the binary glass MD at the same temperature. The open triangles correspond to a normalization of the data without considering bigger $\overline{u^2}$ than a cutoff defined by the variance.

effects. In Fig. 5, we also plot the variance of $P_g(\overline{u^2})$ as a function of $\langle\overline{u^2}\rangle_g^2$. Again we obtain an almost linear behavior, indicating that Eqs. (22) and (26) are valid.

Although the agreement is qualitatively correct between simulations and theory, we observe an asymmetric behavior when compared with Eq. (24). To visualize the asymmetric and the tail of $P_g(\overline{u^2})$, in Fig. 6 we reproduce the same data of Fig. 4 using a semilog scale, where this behavior is more evident when compared with a normal distribution $\mathcal{N}(0,1)$. This behavior is basically due to the fact that in some ISs, the system does not reach the plateau for the given cutoff. Thus, we can normalize the data by using only those $\overline{u^2}$ which are lower than a cutoff defined by the variance, as shown in Fig. 6 with open triangles. The agreement is much better and gives a further refinement of the cutoff criterion. Also in Fig. 6, we see the crystal simulation points and their good agreement with the normal distribution.

We realize that in Eq. (24), $\sigma_g^2 \approx \langle\langle\omega^{-2}\rangle\rangle^2$ appears in the denominator of the exponential decay part. Also, we notice that due to the boson peak, $\langle\langle\omega^{-2}\rangle\rangle > \langle\omega^{-2}\rangle_c$ [35], or in other terms, $\sigma_g^2 > \sigma_c^2$. Then a natural consequence of the boson peak is that $P_c(\overline{u^2})$ decays faster than $P_g(\overline{u^2})$ and therefore the distribution of square displacements in glasses has a long tail at a bigger $\overline{u^2}$. Also, from the simulations we observed that it has a more asymmetric shape than its crystal counterpart. Other effects of the boson peak are seen in some statistical properties of $P_g(\overline{u^2})$ and $P_c(\overline{u^2})$. For example, if we had equivalent glassy and crystalline systems, the mean and variance in the glass would be bigger than in the crystal, i.e.,

$$\langle\overline{u^2}\rangle_g > \langle\overline{u^2}\rangle_c \quad \text{and} \tag{28}$$

$$\sigma_g^2 > \sigma_c^2. \tag{29}$$

Actually, the relation given by Eq. (28) has already been explained through MD simulations in glasses and crystals [35,36]. As a result, in glasses the interbasin dynamics can have a significant overlap with the time scale of harmonic vibrations.

IV. CONCLUSIONS

The aim of this paper is to find the distribution function of the quadratic displacement in crystals and glasses in order to understand what determines the fluctuations in such a quantity. We obtained that inside a MB [16,17], the distribution is given by a Gamma function with a mean that depends linearly on the temperature and on the inverse second moment of the density of vibrational states. The width of the distribution is also dependent on this last quantity. Thus, the boson peak leads to changes in $P(\overline{u^2};l)$ when a glass is already formed. The contribution of the boson peak is evident on the tail of the distribution function (20). It causes the distribution of the MSD to decay slower in glasses than in crystals, and it indicates a different local topology of the energy landscape. When statistics are measured under ISs, we obtain a Gaussian in which the width is regulated by the mean inverse second moment of the density of states. The simulations are only in good qualitative agreement with such a result because the cutoff used does not work for all ISs; however, the analysis of the distribution allows us to further separate the interdynamics and intradynamics by cutting the tail. Finally, it would be interesting to compare the MSD for transitions involving cage-breaking processes with the contributions from low-barrier rearrangements within a metabasin [23,24]. In principle, cage breaking involves a mean-square displacement above a certain threshold [23]. Since glasses have long tails in the distribution of the MSD, the probability for cage-breaking events is increased when compared to crystals. These long tails are a consequence of a reduction in the number of constraints, in agreement with intuitive ideas concerning cage breaking and lack of contacts [25,63].

ACKNOWLEDGMENTS

We thank DGAPA-UNAM projects IN-100310-3. The calculations were performed at Kanbalam and Bakliz supercomputers at DGSCA-UNAM. Hugo M. Flores-Ruiz thanks CONACyT for support through a Ph.D. scholarship.

[1] F. H. Stillinger and T. A. Weber, Science **225**, 983 (1984).
[2] P. Debenedetti and F. Stillinger, Nature (London) **410**, 259 (2001).
[3] J. Langer, Phys. Today **60**(2), 8 (2007).
[4] R. Kerner and G. Naumis, J. Phys.: Condens. Matter **12**, 1641 (2000).
[5] I. Avramov, J. Non-Cryst. Solids **357**, 3841 (2011).

[6] M. M. Smedskjaer, J. C. Mauro, S. Sen, and Y. Yue, Chem. Mater. **22**, 5358 (2010).
[7] M. Goldstein, J. Chem. Phys. **51**, 3728 (1969).
[8] F. H. Stillinger, Science **267**, 1935 (1995).
[9] S. Sastry, P. G. Debenedetti, and F. H. Stillinger, Nature (London) **393**, 554 (1998).
[10] T. B. Schroder, S. Sastry, J. C. Dyre, and S. C. Glotzer, J. Chem. Phys. **112**, 9834 (2000).
[11] F. Sciortino, J. Stat. Mech.: Theor. Exp. (2005) P05015.
[12] P. E. Ramírez-González, L. López-Flores, H. Acuña-Campa, and M. Medina-Noyola, Phys. Rev. Lett. **107**, 155701 (2011).
[13] P. Ramírez-González and M. Medina-Noyola, Phys. Rev. E **82**, 061504 (2010).
[14] M. L. de Haro, J. T. Martínez, L. Gonçalves, and A. Vieira, J. Non-Cryst. Solids **329**, 82 (2003).
[15] K. Broderix, K. K. Bhattacharya, A. Cavagna, A. Zippelius, and I. Giardina, Phys. Rev. Lett. **85**, 5360 (2000).
[16] B. Doliwa and A. Heuer, Phys. Rev. Lett. **91**, 235501 (2003).
[17] B. Doliwa and A. Heuer, Phys. Rev. E **67**, 030501 (2003).
[18] G. A. Appignanesi, J. A. Rodriguez Fris, R. A. Montani, and W. Kob, Phys. Rev. Lett. **96**, 057801 (2006).
[19] O. Rubner and A. Heuer, Phys. Rev. E **78**, 011504 (2008).
[20] Y. Yang and B. Chakraborty, Phys. Rev. E **80**, 011501 (2009).
[21] T. F. Middleton and D. J. Wales, Phys. Rev. B **64**, 024205 (2001).
[22] T. Middleton and D. Wales, J. Chem. Phys. **118**, 4583 (2003).
[23] V. K. de Souza and D. J. Wales, J. Chem. Phys. **129**, 164507 (2008).
[24] V. K. de Souza and D. J. Wales, J. Chem. Phys. **130**, 194508 (2009).
[25] A. S. Kraemer and G. G. Naumis, J. Chem. Phys. **128**, 134516 (2008).
[26] L. Larini, A. Ottochian, C. De Michele, and D. Leporini, Nat. Phys. **4**, 42 (2008).
[27] K. Niss, C. Dalle-Ferrier, B. Frick, D. Russo, J. Dyre, and C. Alba-Simionesco, Phys. Rev. E **82**, 021508 (2010).
[28] C. D. Estrada and M. Robles, J. Chem. Phys. **134**, 044115 (2011).
[29] A. Huerta and G. G. Naumis, Phys. Rev. B **66**, 184204 (2002).
[30] G. G. Naumis, Phys. Rev. B **61**, R9205 (2000).
[31] G. G. Naumis, J. Non-Cryst. Solids **232–234**, 600 (1998).
[32] G. G. Naumis, J. Non-Cryst. Solids **352**, 4865 (2006).
[33] G. G. Naumis, Phys. Rev. B **73**, 172202 (2006).
[34] G. G. Naumis and R. Kerner, J. Non-Cryst. Solids **231**, 111 (1998).
[35] G. G. Naumis and H. M. Flores-Ruiz, Phys. Rev. B **78**, 094203 (2008).
[36] H. M. Flores-Ruiz and G. G. Naumis, J. Chem. Phys. **131**, 154501 (2009).
[37] S. R. Elliot, *Physics of Amorphous Materials*, 2nd ed. (Longman Scientific & Technical, London, 1990).
[38] K. Binder and W. Kob, *Glassy Materials and Disordered Solids* (World Scientific, Singapore, 2005).
[39] H. M. Flores-Ruiz and G. G. Naumis, Phys. Rev. B **83**, 184204 (2011).
[40] K. Trachenko, M. Dove, M. Harris, and V. Heine, J. Phys.: Condens. Matter **12**, 8041 (2000).
[41] J. C. Phillips, J. Non-Cryst. Solids **34**, 153 (1979).
[42] M. Thorpe, J. Non-Cryst. Solids **57**, 205 (1983).
[43] J. Mauro, Am. Ceram. Soc. Bull. **90**, 31 (2011).
[44] M. Bauchy and M. Micoulaut, J. Non-Cryst. Solids **357**, 2530 (2011).
[45] P. Chen, C. Holbrook, P. Boolchand, D. G. Georgiev, K. A. Jackson, and M. Micoulaut, Phys. Rev. B **78**, 224208 (2008).
[46] T. F. Middleton, J. Hernández-Rojas, P. N. Mortenson, and D. J. Wales, Phys. Rev. B **64**, 184201 (2001).
[47] J. Fernandez and P. Harrowell, J. Chem. Phys. **120**, 9222 (2004).
[48] K. Vollmayr, W. Kob, and K. Binder, J. Chem. Phys. **105**, 4714 (1996).
[49] H. M. Flores-Ruiz, G. G. Naumis, and J. C. Phillips, Phys. Rev. B **82**, 214201 (2010).
[50] N. W. Ashcroft and N. D. Mermin, *Solid State Physics* (Harcourt College, Philadelphia, 1976).
[51] J. V. José and E. J. Saletan, *Classical Dynamics: A Contemporary Approach*, 6th printing (Cambridge University Press, New York, 2006).
[52] M. Akkouchi, Soochow J. Math. **31**, 205 (2005).
[53] H. Jasiulewicz and W. Kordecki, Demostratio Mathematica **36**, 231 (2003).
[54] N. L. Johnson, S. Kotz, and N. Balakrishnan, *Continuos Univariate Distributions*, 2nd ed., Vol. 1 (Wiley, New York, 1994).
[55] A. M. Mathai, Ann. Inst. Statist. Math. **34**, 591 (1992).
[56] M. V. Lomonosov, Problem Inform. Transmission **10**, 73 (1974).
[57] L. D. Landau and E. M. Lifshitz, *Física Estadística*, 2nd ed., Vol. 5 (Reverté, Spain, 2002).
[58] J. Wuttke, W. Petry, G. Coddens, and F. Fujara, Phys. Rev. E **52**, 4026 (1995).
[59] D. Engberg, A. Wischnewski, U. Buchenau, L. Borjesson, A. J. Dianoux, A. P. Sokolov, and L. M. Torell, Phys. Rev. B **58**, 9087 (1998).
[60] B. Frick and D. Richter, Phys. Rev. B **47**, 14795 (1993).
[61] R. E. Peierls, Ann. Inst. Henri Poincare **5**, 177 (1935).
[62] S. V. Meshkov, Phys. Rev. B **55**, 12113 (1997).
[63] A. Huerta and G. Naumis, Phys. Lett. A **299**, 660 (2002).